

# Ultra-Slow Throw Rates of Polygonal Fault Systems

James J. King<sup>1</sup>, Joe A. Cartwright<sup>1</sup>

<sup>1</sup>*Department of Earth Sciences, University of Oxford, Oxford OX1 3AN, UK*

## ABSTRACT

Polygonal Fault Systems (PFS) are an enigmatic class of small non-tectonic extensional faults. PFS are predominantly hosted in fine-grained sedimentary tiers and are prevalent along many continental margin basins. The genesis of PFS is widely debated and little is known about the timeframe for polygonal fault growth. We present the first measurements of throw rates for polygonal faults by measuring the vertical offset of seven age-calibrated horizons mapped using three-dimensional seismic reflection data from the Norwegian Sea. Individual polygonal faults exhibit a range of throw rate profiles through time, ranging from near linear to singly or multiply stepped. The stepped profiles have a range of short-term throw rates ranging from 0 to 18 m/Ma. Time-averaged throw rates of 180 polygonal faults over the entire 2.61-0 Ma interval are normally distributed and range between 1.4-10.9 m/Ma. We convert our PFS throw rates to displacement rates and compare these to published displacement rates for gravity driven and tectonic normal faults. We find that the displacement rates of polygonal faults mark the lower limit of a continuous spectrum of extensional fault displacement rates; they are up to two orders-of-magnitude slower than gravity-driven faults, and up to three orders-of-magnitude slower than the fastest growing tectonic faults. We attribute the ultra-slow kinematic behaviour to the non-tectonic nature of polygonal faults where throw accumulates primarily through dewatering of the largely fine-grained sediments comprising the host layers for the PFS, and differential volumetric strain between the fault footwalls and hangingwalls.

## INTRODUCTION

First identified as intra-formational faults within Eocene and Oligocene claystones of Belgium over 30 years ago (Henriet et al., 1988), polygonal faults are now recognised in over 160 basins worldwide, where they often extend over vast areas  $\sim 10^5$ - $10^7$  km<sup>2</sup> (Cartwright et al., 2003; Cartwright, 2011). Polygonal Fault Systems (PFS) have attracted considerable attention in recent years partly because of their ubiquity in many fine-grained slope depositional systems, but also because of their importance as sealing sequences for petroleum, CO<sub>2</sub>, and high grade nuclear waste (Cartwright, 2011). Polygonal faults can also be used to guide the search for deep-water clastic reservoirs (Jackson et al., 2014; Turrini et al., 2017). More fundamentally, PFS are interesting as structures because they are a challenge for classical soil mechanical theory in that they form during early burial, under conditions of net zero lateral strain, yet represent shear failure of unconsolidated granular materials (Shin et al., 2010).

The structural characteristics of PFS are well documented (see Cartwright, 2011 and references therein). PFS are developed in ‘tiers’, as laterally extensive arrays of layer-bound non-tectonic normal faults. These arrays are typically characterised by multi-directional fault patterns in planform, hence the name ‘polygonal fault systems’. Throw profiles on individual polygonal faults are relatively well documented from a number of different PFS and exhibit similar variations to those seen on many small tectonic normal faults, albeit with modified forms due to the complex three-dimensional intersection geometries resulting from the polygonal architecture (Nicol et al., 2003; Stuevold et al., 2003; Neagu et al., 2010; Wrona et al., 2017). An empirical scaling relationship has been suggested for PFS between the maximum throw and the height of a

polygonal fault, where maximum throw values are around 3-6% of the fault height (Shin et al., 2010).

Although the processes that govern the nucleation and propagation of polygonal faults are generally considered to be unrelated to far-field tectonic stresses (Goult, 2008; Cartwright et al., 2003; Verschuren, 2019), there is as yet no agreement on their precise genetic evolution. Suggested mechanisms include gravity sliding, density inversion, overpressure, gravitational loading, and diagenetically-induced shear failure (Cartwright et al., 2003; Goult, 2008; Cartwright, 2011; Verschuren, 2019). Advances in our understanding of PFS have been hindered in part by a scarcity of field outcrop examples to provide sub-seismic observations of the fault zones and associated minor structures (Tewksbury et al., 2014; Verschuren, 2019). An additional, important unconstrained parameter to date has been the lack of any direct measurements of throw rates of polygonal faults.

Here we attempt to bridge this gap in knowledge by presenting the first direct measurements of throw rates for polygonal faults, using an exceptional seismic reflection and well data set from the Norwegian Sea. The key to measuring the throw rates is, firstly, identifying currently active faults, secondly, establishing that they propagated to the seabed at an earlier stage in their evolution, and thirdly, having good age calibration of horizons that are offset by the faults. These criteria are fulfilled by the combination of high-resolution 3D seismic reflection and borehole data collected by the Ocean Drilling Project (ODP). Our results may not be fully representative of the entire spectrum of PFS so far identified globally, but they at least provide direct constraints for those attempting to model the evolution of these extraordinary structures.

## **GEOLOGICAL SETTING**

The study area is located within the Vøring Basin on the outer part of the Norwegian continental margin (Fig. 1A), and extends over a small area of a laterally extensive PFS tier developed within Eocene to Pliocene hemipelagic sediments (Gay & Berndt, 2007; Ireland et al., 2010; Neagu et al., 2010). Previous studies of this PFS in nearby areas have described the detailed geometry of the system and its relationship to the stratigraphy (Hansen et al., 2005; Gay & Berndt, 2007; Ireland et al., 2010; Neagu et al., 2010). The PFS tier is almost uniform in thickness (~1000 m) across the study area (Fig. 1B), but varies in thickness over the rest of the basin. Host strata comprise fine-grained siliceous mudstones and claystones of the Naust, Kai, and Brygge formations, with a prominent Opal A/CT diagenetic phase boundary occurring in the lower third of the tier (Fig. 1B & 1C) (Ireland et al., 2010; Neagu et al., 2010).

## **METHODS**

We mapped the faults and horizons in the study area using two adjoining high-resolution 3D seismic reflection surveys (Fig. 1A). These surveys (SH0701 and BG0904), have a bin spacing of 6.25 m and 25 m, respectively, and a vertical resolution of ~6 m and ~10 m respectively in the uppermost sedimentary interval (see GSA Data Repository, Fig. DR1). We plotted detailed throw profiles for 52 individual polygonal faults by measuring the vertical offset for up to 70 horizons in two way travel time (TWT) (Fig. DR3). We transform the throw versus TWT plots into throw versus geologic age plots using seven bio- and magnetostratigraphic dated marker horizons distributed throughout the 0-2.61 Ma interval, which is the focus of the study. We convert dated marker horizons and formation boundaries from two wells, ODP 644 and 6604/2-

1, to milliseconds TWT from depth in meters, using an internal velocity of 1600 m/s (Eldholm et al., 1987). The uncertainty in the depth conversion of the dated marker horizons on the seismic reflection data equates to +/- 0.1 Ma for horizons <1 Ma and +/-0.2 Ma for horizons >1Ma (for detailed description see GSA Data Repository). Throw measurements of the age-calibrated horizons are considered accurate to +/- 1 m (c.f. Townsend et al., 1998). Time-averaged throw rates are derived from the 2.61 Ma horizon to the present day seabed, by dividing the throw by the elapsed time.

## RESULTS

The base of the PFS tier is identified as the base of the Brygge Formation (Eocene-Oligocene) (Fig. 1B), and >90% of the basal fault tips occur at this horizon. In contrast, there is an upward reduction in fault density and the polygonal fault upper tips terminate at a range of seismic reflections. Only the larger throw faults continue upwards to tip out at or close to the modern seabed (Fig. 1B, 2A, 2B). These polygonal faults have measureable bathymetric expression (Fig. 2A) suggesting continued activity to the present day (c.f. Berndt et al., 2012).

On a small number of the larger faults, reflection-bound intervals thicken noticeably across the faults in a manner typical of localised syn-sedimentary growth (Cartwright et al., 1998; Childs et al., 2003) (Fig. 2C & 2D). These ‘growth packages’ are comparable to those identified elsewhere associated with polygonal faults (e.g. Stuevold et al., 2003; Wrona et al., 2017). They are not found at any specific horizon, but are sporadically distributed throughout the interval corresponding to the last 2.61 Myrs. Average sedimentation rates outpace displacement rates by

at least one order of magnitude during this interval (GSA Data Repository Fig. DR5). This may explain why growth packages are so infrequently developed in the study area.

We constructed throw versus depth plots for 52 widely distributed polygonal faults whose upper tips are at or close to the present day seabed. These plots (GSA Data Repository Fig. DR3) show that throw increases downwards from the seabed to a maximum value in the central to lower third of the tier, and then decreases downwards to the basal tips, in a similar manner to that previously described for polygonal faults (e.g. Neagu et al., 2010). The upper portions of these plots are transformed into throw versus geological age profiles (Fig. 3A), whose gradient changes reveal temporal changes in throw rate (Fig. 3A, DR4).

Individual faults exhibit a range of profiles of throw with time, from almost linear profiles (constant throw rate with time, e.g. Fig. 3A, PF\_037) to singly or multiply stepped (variable throw rate through time with zero gradient stasis intervals, e.g. Fig 3A, PF\_029). Of the 52 faults, around 60% of profiles are approximately linear, or smoothly varying, and the remainder are stepped (Fig. 3A). The stepped profiles exhibit a range of short-term throw rates ranging from 0 to 18 m/Ma.

In addition to the detailed throw versus age profiles, we derive time-averaged throw rates from a larger sample of 180 individual faults for the entire 2.61-0 Ma interval (Fig. 3B). The measured throw rates are normally distributed and range between 1.4-10.9 m/Ma, with a mean and median of 5.7 m/Ma and 5.6 m/Ma respectively.

## DISCUSSION

In order to measure throw rates for faults from upper tip geometries of the type presented above, it must be clear that the upper tips propagated in a syn-sedimentary fashion, i.e. with the tip at or close to the sediment-water interface (Childs et al., 2003; Baudon & Cartwright, 2008). The throw rate data presented here all come from polygonal faults with upper tips at or within a few metres of the current seabed. The occurrence of small ‘growth packages’ within the age-calibrated stratigraphy (Fig. 2C, 2D), albeit infrequent, and the presence of polygonal faults at or within a few meters of the modern seabed (Fig. 1B, 2A, 2B) indicates that the upper tips of the PFS have intersected the paleo-seabed throughout our chronostratigraphic study interval, and propagated upwards with sedimentation in an active syn-sedimentary fashion. This interpretation is consistent with that of Neagu et al., (2010), who dated fault activity on this PFS in relation to the fossilisation of the Opal A to Opal CT diagenetic boundary. Neagu et al., (2010) used measured throw values of the Opal A/CT to argue for a post-fossilisation syn-sedimentary growth phase for the PFS in the Norwegian Sea. They dated the fossilisation as Late Miocene to Early Pliocene, which accords well with the oldest dated horizon in our study (2.61 Ma). Furthermore, we interpret stasis intervals across different polygonal fault throw profiles (Fig. 3A) as short periods of growth inactivity, rather than the mechanical response to blind fault propagation through competent stratigraphy, because of their non-systematic occurrence relative to stratigraphic layering. It is possible that the PFS may have nucleated and propagated as an array of blind faults that became syn-sedimentary later in the evolution of the system (c.f. Baudon & Cartwright, 2008). Whilst we cannot rule out the possibility that some polygonal faults may have propagated to their current position as blind faults we consider it is unlikely that the polygonal faults analysed in our study were blind faults over the last 2.61 Myrs.

The measured throw rates both for short time increments and for the entire 2.61 Myr period of the measured interval give comparable ranges in values, from 0 to 18 m /Ma (Fig. 3B, DR4). To make a comparison with previously measured fault displacement rates, we can convert our throw rates to displacement rates if we assume that displacement vectors are dip-slip, and by knowing the true dip of the fault planes. This correction factor amounts to 1.1 to 1.4 for faults dipping between 45-70°. Displacement rates for these polygonal faults compared to basement detached, gravity-driven, and tectonic faults from various rift settings shows that polygonal faults slip one to three orders of magnitude more slowly (time averaged) than their tectonic counterparts (Fig. 4). Our derived PFS displacement rates are the lowest ever measured for a fault array of any type globally. This comparison prompts interesting questions as to the slip mechanism: do polygonal faults creep or do they exhibit stick-slip behaviour as has been suggested (Tewksbury et al., 2014)?

Regardless of the underlying genetic mechanism, the accommodation of multi-directional extensional faults under net-zero lateral strain conditions requires a bulk volumetric reduction of the host tier. It is beyond the scope of the current study to attempt to explain the very slow slipping behaviour of polygonal faults. However, the ultra-slow nature of polygonal faults is not a complete surprise given the slow rates of geological processes that govern volumetric reductions in shallowly buried fine-grained sediments. These slow geological processes may include the rate of gravitational loading through sedimentation in deep-marine pelagic depositional environments, the rate of dewatering in low-permeability fine-grained sediments, and the rate of low temperature diagenetic reactions (Goult, 2008; Cartwright, 2011). The



negative throw gradients observed on the lower portions of t-z plots of all polygonal faults measured to date strongly argues that there is a differential volumetric strain from footwall relative to hangingwall that accounts for a large part, if not all, of the displacement that accumulates along the fault throughout its growth history. We suggest that the ultra-slow rates presented in this study, point to a direct link between the displacement rate and the differential volumetric contractional strain rate between the footwall and hangingwall. This differential is in turn likely to be governed by bulk material properties such as stiffness, Poisson's ratio, and frictional coefficients (Shin et al., 2010; Roberts et al., 2014).

In isolation, the ultra-slow displacement rates do not explicitly favour one PFS genetic or growth mechanism over another. They do however, offer an initial temporal benchmark that may assist future computational modelling work to establish the physical property conditions and mechanical evolution building on some pioneering attempts to model growth of polygonal faults using finite element methods (Roberts et al., 2014).

## CONCLUSIONS

1. We record the first throw rates for a polygonal fault system, from the Vøring Basin in the Norwegian Sea.
2. Our results from 180 polygonal faults show that time-averaged throw rates over the last 2.61 Myrs are normally distributed and range between 1.4-10.9 m/Ma.
3. Our derived PFS displacement rates mark the lower limit of a continuous spectrum of extensional fault displacement rates, where the displacement rates of polygonal faults are up to three orders of magnitude slower than the fastest-growing tectonic faults.

4. The ultra-slow PFS throw rates are consistent with slow geological processes that drive differential bulk volumetric reductions between fault footwalls and hangingwalls.

## ACKNOWLEDGEMENTS

NERC (NE/M00578X/1) and the Oxford-Radcliffe Scholarship are thanked for funding. We thank Schlumberger for providing a Petrel license. Seismic data was provided by Norske Shell A/S. We thank B. Tewksbury, C. Jackson, and S. Sonnenberg for insightful reviews, and M. Foschi, D. James, C. Kirkham, and B. Levell for helpful discussion.

## REFERENCES CITED

- Baudon, C., & Cartwright, J. (2008). Early stage evolution of growth faults: 3D seismic insights from the Levant Basin, Eastern Mediterranean. *Journal of Structural Geology*, 30(7), 888-898. doi.org/10.1016/j.jsg.2008.02.019
- Berndt, C., Jacobs, C., Evans, A., Gay, A., Elliott, G., Long, D., & Hitchen, K. (2012). Kilometre-scale polygonal seabed depressions in the Hatton Basin, NE Atlantic Ocean: Constraints on the origin of polygonal faulting. *Marine Geology*, 332, 126-133. doi.org/10.1016/j.margeo.2012.09.013
- Cartwright, J., Bouroullec, R., James, D., & Johnson, H. (1998). Polycyclic motion history of some Gulf Coast growth faults from high-resolution displacement analysis. *Geology*, 26(9), 819-822. doi.org/10.1130/0091-7613(1998)026<0819:PMHOSG>2.3.CO;2
- Cartwright, J., James, D., & Bolton, A. (2003). The genesis of polygonal fault systems: a review. Geological Society, London, Special Publications, 216(1), 223-243. doi.org/10.1144/GSL.SP.2003.216.01.15

230 Cartwright, J. (2011). Diagenetically induced shear failure of fine-grained sediments and the  
 231 development of polygonal fault systems. *Marine and Petroleum Geology*.  
 232 doi.org/10.1016/j.marpetgeo.2011.06.004.

233 Childs, C., Nicol, A., Walsh, J. J., & Watterson, J. (2003). The growth and propagation of  
 234 synsedimentary faults. *Journal of Structural geology*, 25(4), 633-648.  
 235 doi.org/10.1016/S0191-8141(02)00054-8

236 Dutton, D. M., & Trudgill, B. D. (2009). Four-dimensional analysis of the Sembo relay system,  
 237 offshore Angola: Implications for fault growth in salt-detached settings. *AAPG Bulletin*,  
 238 93(6), 763–794. doi.org/10.1306/02230908094.

239 Eldholm, O., Thiede, J., Taylor, E. (1987). Site 644: Norwegian Sea. In *Proceedings of the*  
 240 *Ocean Drilling Program, 104 Initial Reports*. Ocean Drilling Program.  
 241 doi.org/10.2973/odp.proc.ir.104.105.1987.

242 Gay, A., & Berndt, C. (2007). Cessation/reactivation of polygonal faulting and effects on fluid  
 243 flow in the Vøring Basin, Norwegian Margin. *Journal of the Geological Society*, 164(1),  
 244 129-141. doi.org/10.1144/0016-76492005-178

245 Goult, N. R. (2008). Geomechanics of polygonal fault systems: a review. *Petroleum*  
 246 *Geoscience*, 14(4), 389-397. doi.org/10.1144/1354-079308-781

247 Hansen, J. P. V., Cartwright, J. A., Huuse, M., & Clausen, O. R. (2005). 3D seismic expression  
 248 of fluid migration and mud remobilization on the Gjallar Ridge, offshore mid-  
 249 Norway. *Basin Research*, 17(1), 123-139. doi.org/10.1111/j.1365-2117.2005.00257.x

250 Henriot, J. P., De Batist, M., Van Vaerenbergh, W., & Verschuren, M. (1988). Seismic facies and  
 251 clay tectonic features of the Ypresian clay in the southern North Sea. *Bulletin van de*  
 252 *Belgische Vereniging voor Geologie*, 97, 457-472.

253 Ireland, M. T., Goult, N. R., & Davies, R. J. (2010). Influence of pore water chemistry on silica  
254 diagenesis: evidence from the interaction of diagenetic reaction zones with polygonal fault  
255 systems. *Journal of the Geological Society*, 167(2), 273–279. doi.org/10.1144/0016-  
256 76492009-049.

257 Jackson, C. A. L., Carruthers, D. T., Mahlo, S. N., & Briggs, O. (2014). Can polygonal faults  
258 help locate deep-water reservoirs?. *AAPG Bulletin*, 98(9), 1717-1738.  
259 doi.org/10.1306/03131413104

260 Jackson, C. A. L. (2018). Throw Rate Variability on Gravity-Driven Normal Faults; Constraints  
261 from the Gudrun Fault, South Viking Graben, Offshore Norway.  
262 doi.org/10.1306/13652189M1153254.

263 Mouslopoulou, V., Walsh, J. J., & Nicol, A. (2009). Fault displacement rates on a range of  
264 timescales. *Earth and Planetary Science Letters*, 278(3-4), 186–197.  
265 doi.org/10.1016/j.epsl.2008.11.031.

266 Neagu, R. C., Cartwright, J., & Davies, R. (2010). Measurement of diagenetic compaction strain  
267 from quantitative analysis of fault plane dip. *Journal of Structural Geology*, 32(5), 641–655.  
268 doi.org/10.1016/j.jsg.2010.03.010.

269 Nicol, A., Walsh, J. J., Watterson, J., & Underhill, J. R. (1997). Displacement rates of normal  
270 faults. *Nature*, 390, 157–159. doi.org/10.1038/36548.

271 Nicol, A., Walsh, J. J., Watterson, J., Nell, P. A. R., & Bretan, P. (2003). The geometry, growth  
272 and linkage of faults within a polygonal fault system from South Australia. *Geological*  
273 *Society, London, Special Publications*, 216(1), 245-261.  
274 doi.org/10.1144/GSL.SP.2003.216.01.16

275 Pochat, S., Castelltort, S., Choblet, G., & Van Den Driessche, J. (2009). High-resolution record  
 276 of tectonic and sedimentary processes in growth strata. *Marine and Petroleum Geology*,  
 277 26(8), 1350–1364. doi.org/10.1016/j.marpetgeo.2009.06.001.

278 Roberts, D. T., Crook, A. J. L., Cartwright, J. A., Profit, M. L., & Rance, J. M. (2014, August).  
 279 The evolution of polygonal fault systems: Insights from geomechanical forward modeling.  
 280 In 48th US Rock Mechanics/Geomechanics Symposium. American Rock Mechanics  
 281 Association.

282 Shin, H., Santamarina, J. C., & Cartwright, J. A. (2010). Displacement field in contraction-driven  
 283 faults. *Journal of Geophysical Research: Solid Earth*, 115(7), 1–13.  
 284 doi.org/10.1029/2009JB006572.

285 Stuevold, L. M., Faereth, R. B., Arnesen, L., Cartwright, J., & Möller, N. (2003). Polygonal  
 286 faults in the Ormen Lange field, Møre basin, offshore mid Norway. Geological Society,  
 287 London, Special Publications, 216(1), 263-281. doi.org/10.1144/GSL.SP.2003.216.01.17

288 Tewksbury, B. J., Hogan, J. P., Kattenhorn, S. A., Mehrkens, C. J., & Tarabees, E. A. (2014).  
 289 Polygonal faults in chalk: Insights from extensive exposures of the Khoman Formation,  
 290 Western Desert, Egypt. *Geology*, 42(6), 479-482. doi.org/10.1130/G35362.1

291 Townsend, C., Firth, I. R., Westerman, R., Kirkevollen, L., Hårde, M., & Andersen, T. (1998).  
 292 Small seismic-scale fault identification and mapping. Geological Society, London, Special  
 293 Publications, 147(1), 1-25. doi.org/10.1144/GSL.SP.1998.147.01.02

294 Turrini, L., Jackson, C. A., & Thompson, P. (2017). Seal rock deformation by polygonal  
 295 faulting, offshore Uruguay. *Marine and Petroleum Geology*, 86, 892-907.  
 296 doi.org/10.1016/j.marpetgeo.2017.06.038

Verschuren, M. (2019). Outcrop evidence of polygonal faulting in Ypresian marine clays (Southern North Sea Basin) leads to a new synthesis. *Marine Geology*, 413, 85-98. doi.org/10.1016/j.margeo.2019.04.002

Wrona, T., Magee, C., Jackson, C. A., Huuse, M., & Taylor, K. G. (2017). Kinematics of polygonal fault systems: observations from the northern North Sea. *Frontiers in Earth Science*, 5, 101. doi.org/10.3389/feart.2017.00101

**Figure 1:** (A) Map of the study area located in the Vøring Basin of the Norwegian Sea, that includes two 3D seismic reflection volumes, SH0701 and BG0904, that are litho- and chronostratigraphically calibrated by two industry wells and ODP 644. (B) A seismic profile of the PFS tier through ODP 644 and 6604/2-1 showing the dated horizons (from Eldholm et al., 1987) used in our analysis, alongside the stratigraphic formation boundaries, and the diagenetic Opal A/CT phase boundary. (C) Stratigraphic column of the PFS host sediments.

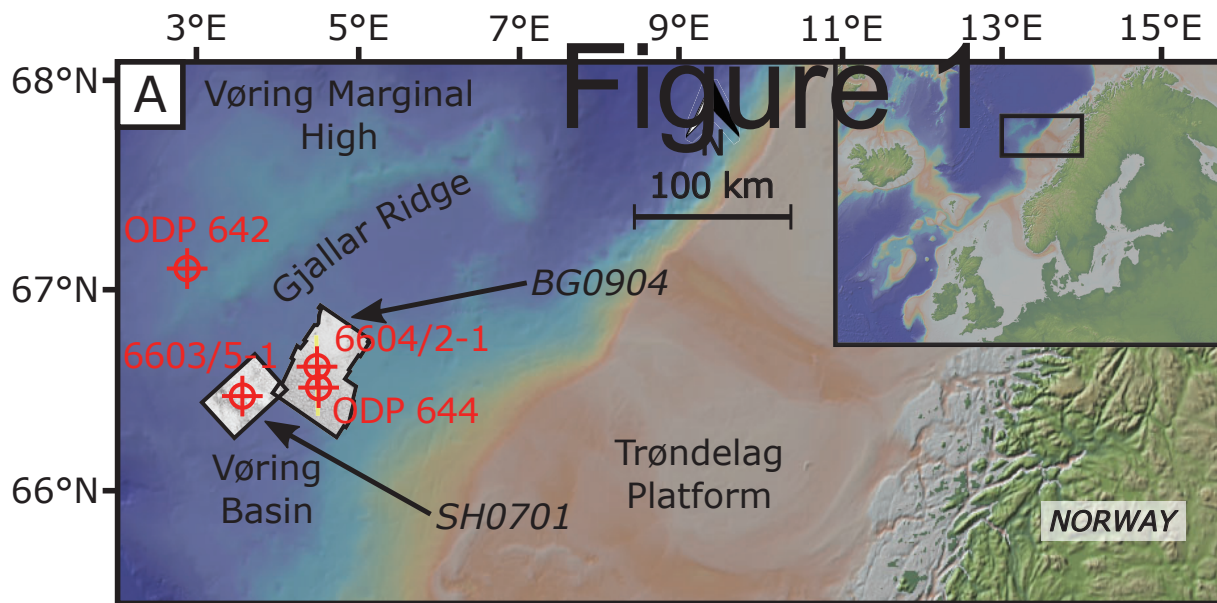
**Figure 2:** (A) Seabed variance map showing the bathymetric expression of polygonal faults. (B) Seismic cross-section showing the bathymetric expression of polygonal fault upper tips (vertical exaggeration ~x15). Faults tips are labelled FT. (C & D) Syn-sedimentary growth package within the age-calibrated stratigraphy.

**Figure 3:** (A) Polygonal fault throw versus horizon age for 14 polygonal fault upper tips. (B) Probability density function of time-averaged PFS throw rates derived from the 2.61 Ma horizon for 180 faults.

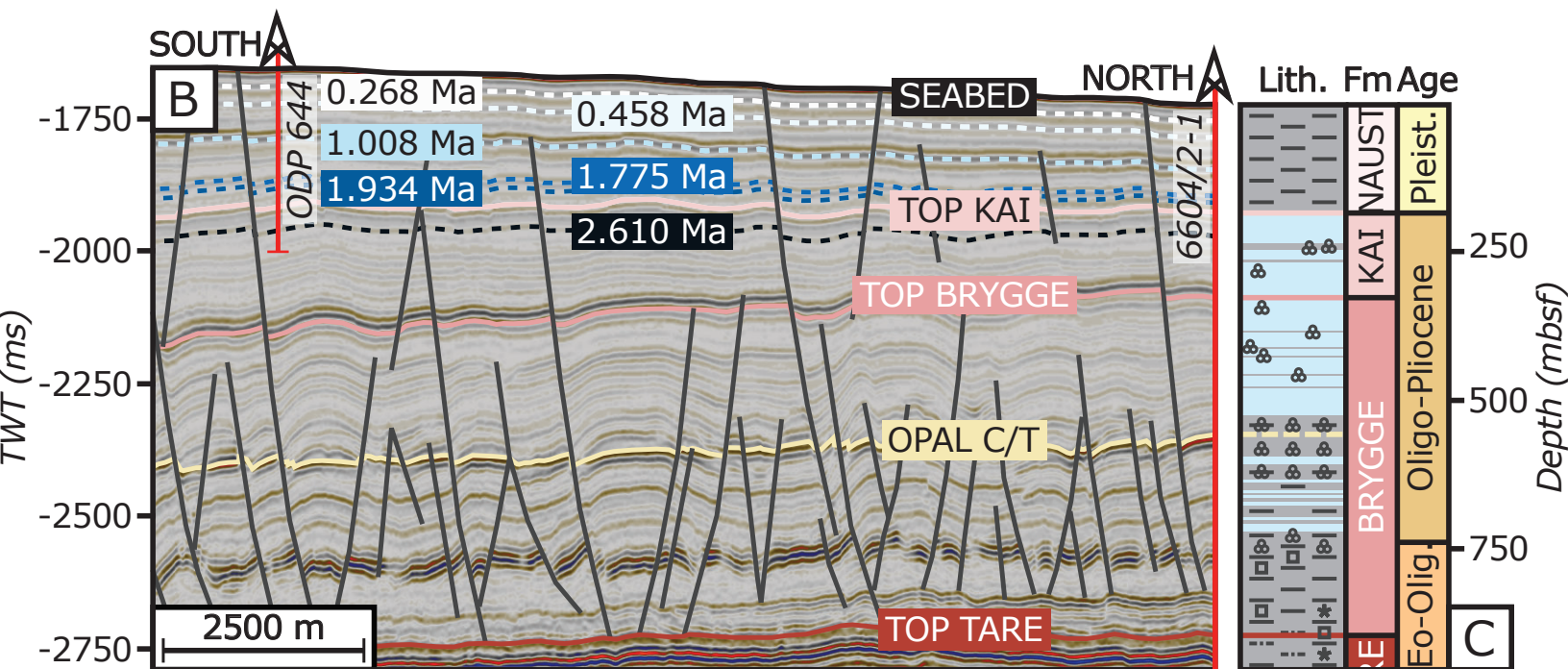
**Figure 4:** Log plot of displacement rates from extensional tectonic, gravity-driven, and polygonal fault systems from basins around the world. Tectonic and gravity-driven fault displacement rates sourced from; Nicol et al., (1997); Mouslopoulou et al., (2009); Dutton & Trudgill (2009); Pochat et al., (2009); Jackson (2018). PFS time-averaged throw rates are converted to displacement rates using a conversion factor of 1.4.



# Figure 1



**Strat Column Legend**





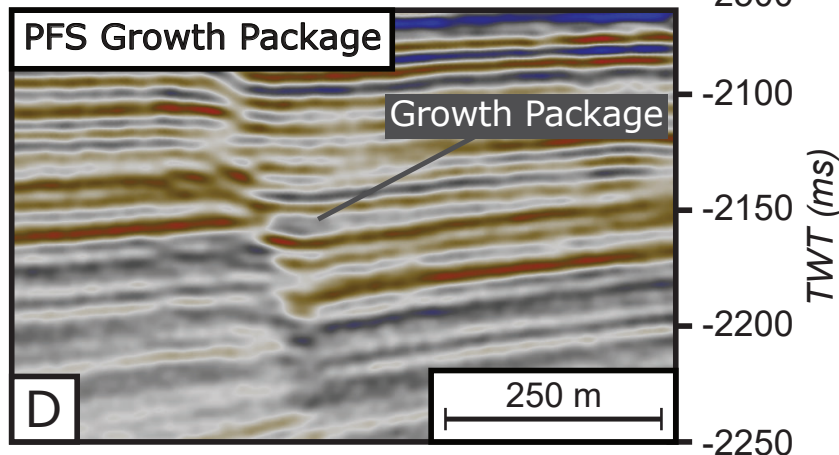
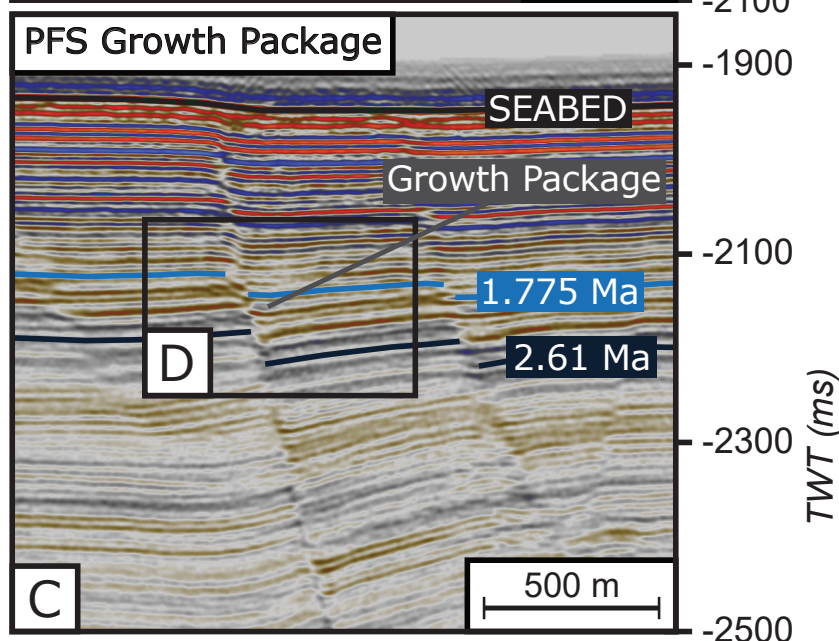
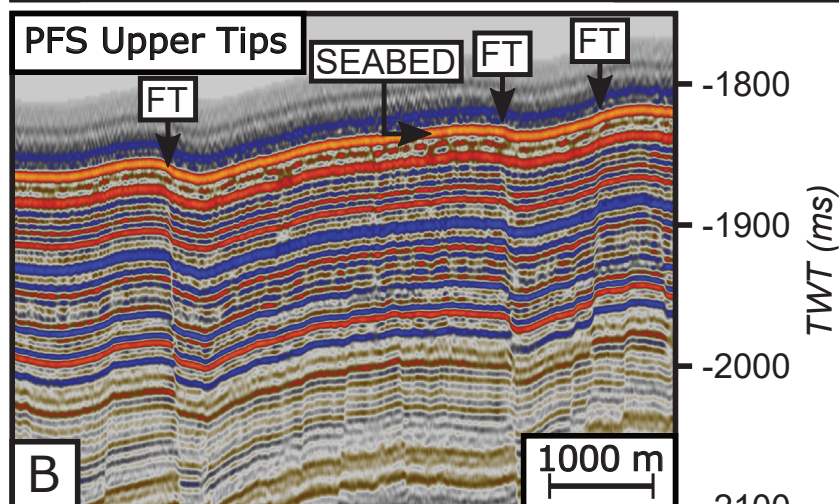
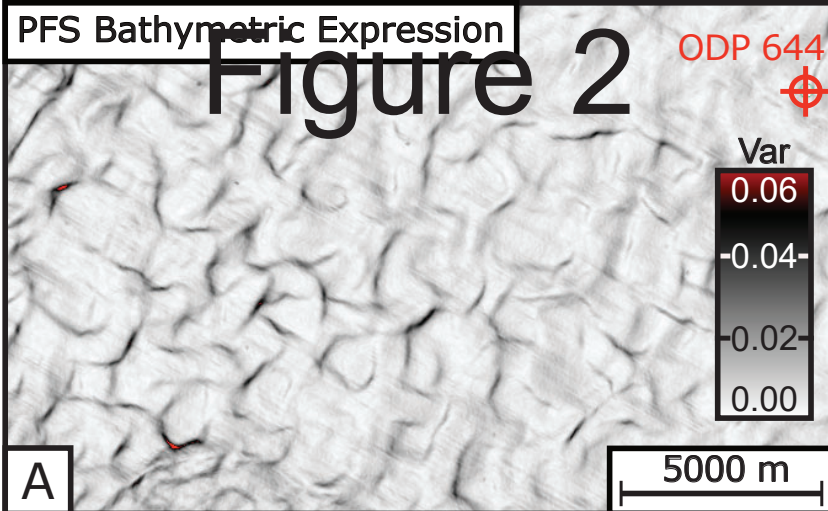


# Figure 3

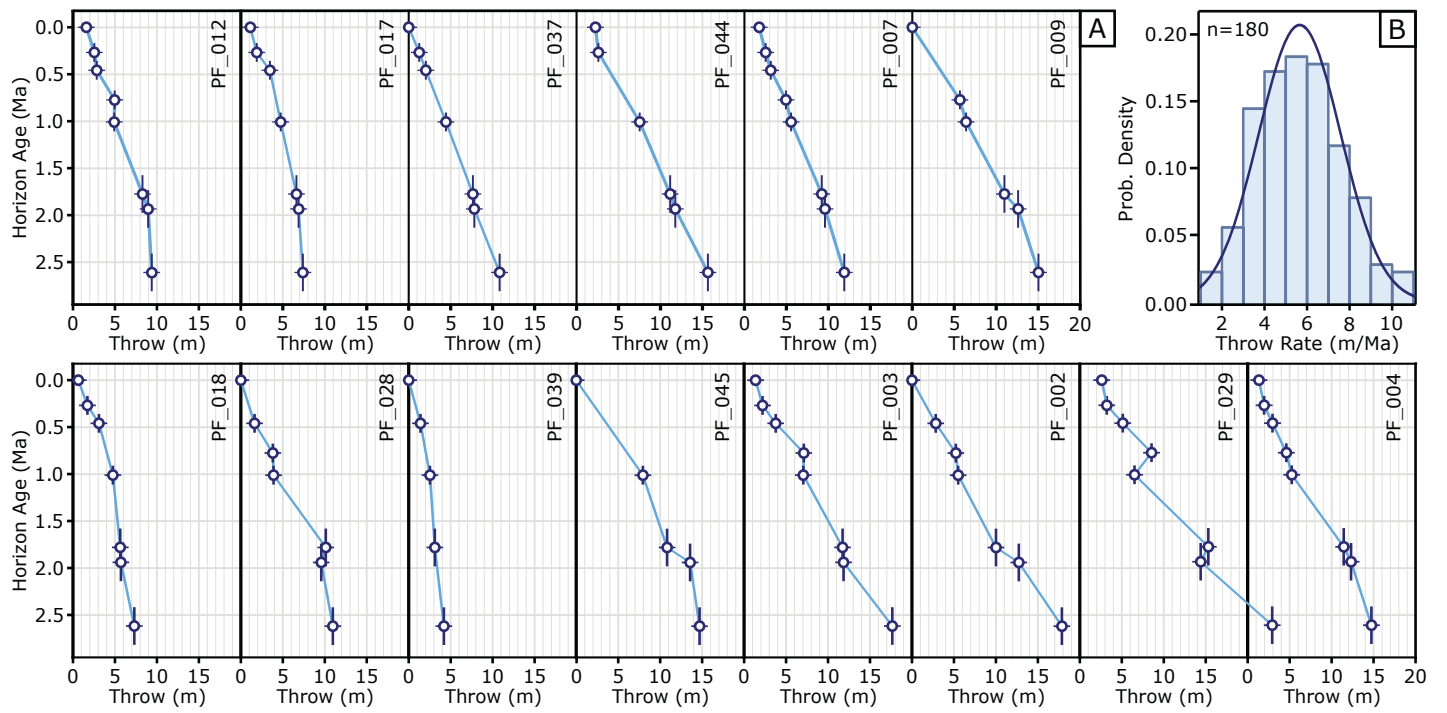


# Figure 4

